Estimates of the Regional Distribution of Sea Level Rise over the 1950–2000 Period

JOHN A. CHURCH AND NEIL J. WHITE

CSIRO Marine Research and Antarctic Climate and Ecosystems Cooperative Research Centre, Hobart, Tasmania, Australia

RICHARD COLEMAN

Department of Geomatics, University of Tasmania, and CSIRO Marine Research, Hobart, Tasmania, Australia

KURT LAMBECK

Research School of Earth Sciences, Australian National University, Canberra, Australian Capital Territory, Australia

JERRY X. MITROVICA

Department of Physics, University of Toronto, Toronto, Ontario, Canada

(Manuscript received 15 July 2003, in final form 12 January 2004)

ABSTRACT

TOPEX/Poseidon satellite altimeter data are used to estimate global empirical orthogonal functions that are then combined with historical tide gauge data to estimate monthly distributions of large-scale sea level variability and change over the period 1950–2000. The reconstruction is an attempt to narrow the current broad range of sea level rise estimates, to identify any pattern of regional sea level rise, and to determine any variation in the rate of sea level rise over the 51-yr period. The computed rate of global-averaged sea level rise from the reconstructed monthly time series is 1.8 ± 0.3 mm yr^{-1}. With the decadal variability in the computed global mean sea level, it is not possible to detect a significant increase in the rate of sea level rise over the period 1950–2000. A regional pattern of sea level rise is identified. The maximum sea level rise is in the eastern off-equatorial Pacific and there is a minimum along the equator, in the western Pacific, and in the eastern Indian Ocean. A greater rate of sea level rise on the eastern North American coast compared with the United Kingdom and the Scandinavian peninsula is also found. The major sources of uncertainty are the inadequate historical distribution of tide gauges, particularly in the Southern Hemisphere, inadequate information on tide gauge signals from processes such as postglacial rebound and tectonic activity, and the short satellite altimeter record available to estimate global sea level covariance functions. The results demonstrate that tide gauge records will continue to complement satellite altimeter records for observing and understanding sea level change.

1. Introduction

Since the last glacial maximum about 20 000 yr ago, global-averaged sea level has risen by more than 100 m as large ice sheets melted. Most of the rise occurred more than 6000 yr ago. These large transfers of mass from the ice sheets to the oceans change the surface loading of the earth and result in ongoing vertical movement [glacial isostatic adjustment, (GIA)] of the earth's crust and sea surface (see, e.g., Lambeck and Johnston 1998; Peltier 1998; Milne et al. 2001). Estimates of rates of global-averaged sea level rise over the last 1000 yr or so and prior to the twentieth century are less than 0.2 mm yr^{-1} (Fleming et al. 1998; Lambeck and Bard 2000; Lambeck 2002).

Corresponding author address: John Church, CSIRO Marine Research, GPO Box 1538, Hobart, TAS 7001, Australia.
E-mail: john.church@csiro.au

Estimates of twentieth century sea level rise are primarily based on the historical tide gauge data maintained by the Permanent Service for Mean Sea Level (PSMSL; Woodworth and Player 2003). Tide gauges measure the height of the sea surface relative to coastal benchmarks. However, these measurements include a signal from large spatial-scale secular trends in GIA and possibly also tectonic motions, which often occur at smaller spatial scales. To estimate the change in eustatic sea level (i.e., changes in the volume of the ocean), the tide gauge records must be corrected for ongoing GIA and tectonic motions. To date, the only practical way of doing this correction is the use of geological data to infer long-term motions or geophysical models to estimate the GIA. Measurements using a global positioning system (GPS), as presently done in the Baseline Inferences for Fennoscandian Rebound Observations, Sea-level and Tectonics (BIFROST) experiment in

Scandanavia (Johansson et al. 2002) and the South Pacific Sea Level and Climate Monitoring Project (information online at http://www.pacificsealevel.org/), are beginning to provide accurate, direct measurement of vertical land motions at tide gauges.

Estimates of the twentieth century rate of eustatic sea level rise are 1–2 mm yr^{-1}, significantly larger than rates over the last several centuries. Douglas (1997) estimated a rate of global-averaged sea level rise of 1.8 $\pm$ 0.1 mm yr^{-1} using 24 long tide gauge records and the GIA model of Tushingham and Peltier (1991). Using his most recent GIA model and essentially the same gauges as used by Douglas, Peltier's (2001) estimate is 1.84–1.91 mm yr^{-1}. Regional estimates of eustatic sea level rise give a broader range of results. Woodworth et al. (1999) estimated a rate of about 1 mm yr^{-1} for the North Sea region. For Fennoscandinavia, Lambeck et al. (1998b) estimated an average regional rate of 1.1 $\pm$ 0.2 mm yr^{-1}. Estimates for Fennoscandia from the BIFROST program yield a regional rate of eustatic sea level rise of 1.9 $\pm$ 0.2 mm yr^{-1} (Johannsson et al. 2002). For the North American east coast, Gornitz (1995) and Davis and Mitrovica (1996) estimated 1.5 mm yr^{-1} while Peltier (1996) estimated 1.9 $\pm$ 0.6 mm yr^{-1}. Lambeck (2002) estimated sea level rise for the two longest Australian records (Sydney on the east coast and Perth on the west coast) as 1.16 and 1.65 mm yr^{-1} and that sea level records for northwestern Australia indicated a fall in sea level over the last 30 yr. Hunter et al. (2003) found an average rate of sea level rise over 160 yr of 1.0 $\pm$ 0.3 mm yr^{-1} at Port Arthur on the southeast tip of Tasmania, Australia. Zhen and Wu (1993) estimated relative rates of sea level rise in China of 0.5 mm yr^{-1} in the north and about 2 mm yr^{-1} in the south. Mitrovica and Davis (1995) pointed out that the *range* of local GIA corrections may be as much as 0.5 mm yr^{-1} (i.e., $\pm$0.25 mm yr^{-1}) in the far field as a result of poorly known profiles of mantle viscosity. But recent developments in both the theory and the definition of GIA model parameters have led to better results.

Church et al. (2001) and Lambeck (2002) suggested that regional variations in the rate of sea level rise may explain some of these differences. Indeed, regional variations are to be expected with climate change (whether natural or anthropogenic) as air–sea fluxes of momentum, heat, and freshwater change (Gregory et al. 2001). Support for regional variations in sea level rise comes from estimates of ocean thermal expansion for the period 1955–95 (Antonov et al. 2002; Cabanes et al. 2001). Mitrovica et al. (2001b) (see also Nakiboglu and Lambeck 1991) emphasized that recent melting of global ice reservoirs will lead to significant geographic variations in the sea level change due to both gravitational and loading effects. They demonstrated that the lower rates of sea level rise observed at European gauges could be reconciled by the fingerprint of Greenland melting and also estimated an average global mean sea level rise of 1.7 mm yr^{-1}.

For the gauges with the longest record, there is a geographic bias with many more records in the Northern Hemisphere (particularly the North Atlantic) than in the Southern Hemisphere. Cabanes et al. (2001) suggest this geographical bias resulted in a significant overestimate of twentieth century sea level rise. To date no increase in the rate of sea level rise has been detected for the twentieth century (Woodworth 1990; Douglas 1992) although the longest records do indicate an increase in the rate of sea level rise over the last two to three centuries (Woodworth 1999).

Satellite altimetry provides near-global coverage of the world's oceans and thus the promise of determining the global-averaged sea level rise, its regional variations, and changes in the rate of rise more accurately and quickly than is possible from the sparse array of in situ gauges. The altimeter measures change in the geocentric position of sea level whereas we use the tide gauges to estimate eustatic sea level change. Just as estimates of eustatic sea level change from tide gauge records are corrected for the signal due to GIA, analyses of satellite altimetry data need to be corrected for secular changes in the sea surface (geocentric sea level) due to GIA. Numerical predictions of the latter have recently been published (Mitrovica et al. 2001b; Douglas and Peltier 2002). Douglas and Peltier (2002) estimate, using the ICE-4G (VM2) GIA model, that the GIA correction to satellite estimates of sea surface rates will increase the latter by 0.3 mm yr^{-1}. M.E. Tamisiea et al. (2004, unpublished manuscript, hereafter TMLNM) show that this correction ranges from 0.2 to 0.5 mm yr^{-1} when account is taken of uncertanties in the GIA model.

The use of TOPEX/Poseidon satellite altimeter mission [launched in August 1992; Fu and Cazenave (2001)] data to measure sea level rise has improved markedly as small drifts in the satellite system have been revealed by careful comparison of the satellite observations with in situ data (Mitchum 1998, 2000; Cazenave et al. 1999). Estimates of the rates of rise from the short TOPEX/Poseidon record (see Nerem and Mitchum 2001 for a recent review) are 2.5 $\pm$ 1.3 mm yr^{-1} over the 6-yr period 1993–98 (inclusive). Whether this larger estimate is a result of an increase in the rate of rise, systematic errors in the satellite and/or in situ records, the shortness of the satellite record, or a reflection of the large error bars (principally from poorly known vertical land motions of tide gauges used to determine the absolute bias drift of the altimeter) is not clear.

Here, we attempt to improve our understanding of sea level rise by combining the benefits of the short but virtually complete global coverage offered by satellite altimetry with the relatively long but spatially sparse in situ tide gauge dataset. We attempt to achieve three objectives: 1) to narrow the current broad range of sea level rise estimates, 2) to identify any pattern of regional sea level rise, and 3) to determine any variation in the rate of sea level rise between 1950 and 2000.

Our approach differs from the usual attempts to de-

termine sea level rise from tide gauge records. Rather than determining sea level rise from a few long records as exemplified by the studies of Douglas (1991, 1997), we use as many gauges as possible to estimate the global distribution of sea level for each month/year between 1950 and 2000. That is, rather than average out climate variability by using long records, we attempt to explicitly account for this variability, as in the satellite altimeter measurements. The approach is similar to attempts to reconstruct global surface temperatures over similar and longer periods (Smith et al. 1996, 1998; Kaplan et al. 1997, 1998, 2000) and interannual variations in sea level (Chambers et al. 2002). We build on the work of Chambers et al. (2002) by using the near-global coverage from satellite altimetry to estimate the global covariance structure of observed sea level variability and use this information to interpolate the relatively sparse but longer tide gauge records.

In section 2, we describe the datasets and the preliminary processing. The methods for making global reconstructions of sea surface height fields use the optimal interpolation technique developed by Kaplan et al. (1997, 1998, 2000; section 3). We also use a modification of the projection technique used by Smith et al. (1996) for sea surface temperature and Smith (2000) and Chambers et al. (2002) for sea level. Because of the unknown tide gauge datums, we solve for *changes* in sea level between subsequent time steps and then integrate these changes over time to get changes in sea level over the 51-yr period. The reconstructed sea levels compare favorably with the TOPEX/Poseidon satellite altimeter results (section 4). We then present the results of our reconstruction over the period 1950–2000 and discuss the robustness of these results (section 5). The interpretation of the results and the comparison with other findings are discussed in section 6.

2. The datasets and the initial processing

a. The tide gauge dataset

The central dataset we use for the period 1950–2000 is monthly mean sea levels from the data archive of the PSMSL (Woodworth and Player 2003). We use primarily the Revised Local Reference (RLR) data but also some metric data, downloaded from the PSMSL Web site (http://www.pol.ac.uk/psmsl/) in February 2003. The most recent data were for 2002 but for many stations the data end before 2000. The RLR data files are supported by documentation relating measured sea level at each site to a constant local datum over the complete record. The metric records can have substantial and unknown datum shifts and their use in time series analysis is generally not recommended. However, sometimes the metric data are also related to a constant local datum but supporting documentation is lacking at PSMSL.

The metric dataset contains 1950 stations and the RLR dataset 1159 stations, but all RLR stations are included in the metric dataset. We filled gaps of 1–2 months (by spline interpolation) and deleted continuous sections shorter than 2 yr, eliminating 256 records. Where there were both RLR and metric records for stations, the redundant metric record was deleted (1063 records). We also deleted records for 95 locations beyond the TOPEX/Poseidon latitude range and 37 records more than 250 km from the nearest altimeter grid point. This left a total of 1658 records for further assessment. We then removed locations where there was serious disagreement between nearby records, where the gauges were in unsuitable locations (e.g., in an estuary, especially when there was another gauge closer to the ocean), where the records were too fragmented or noisy to be useful, or where there were large residual trends (greater than 10 mm yr^{-1}).

It is not possible to reliably locate the stations in a single consistent vertical reference frame. Therefore, the data we use for analysis are first differences from one month to the next in each of the time series. Records were broken into separate sections, automatically at jumps of greater than 250 mm between adjacent monthly values, and manually at a few (51) more places. These jumps were thought to relate to datum shifts and occurred mostly in the metric records.

As the TOPEX/Poseidon altimeter data used are on a $1° \times 1°$ grid, we found the nearest such grid point for each tide gauge. Where there were multiple tide gauges for a single grid point, the change in height at each time step were averaged to produce a single time series. A total of 945 records (670 RLR and 275 metric) are combined into 454 composite records, of which 426 have useful data in the time span from January 1950 through to December 2000. The number of these composite locations that passed our quality control checks is 154 in 1950, rises to more than 240 prior to 1960, peaks at 317 in 1986 before falling rapidly in the last 5 yr to 196 in 2000 (Fig. 1a). The regional distribution of the gauges (Figs. 1b–f) clearly demonstrates the largest density of gauges is in the North Atlantic and North Pacific Oceans, particularly in the 1950s. Even in the 1980s, noticeable gaps remain in sea level data for the Southern Ocean, the South Atlantic Ocean, and the western Indian Ocean.

The PSMSL sea level data are *relative* sea level. To remove the ongoing GIA, we use the results of three different models. Estimates of these ongoing GIAs are based on the solution of the ''sea level equation'' (Farrell and Clark 1976), which requires two inputs: a rheological model for the earth's viscoelastic response and the space–time history of Late Pleistocene and early Holocene ice cover. The GIA predictions treat the earth as spherically symmetric and self-gravitating, with a layered Maxwell viscoelastic rheology. The density and elastic structure of the earth model are given by the Preliminary Reference Earth Model (PREM; Dziewonski and Anderson 1981) seismic model. The Mitrovica

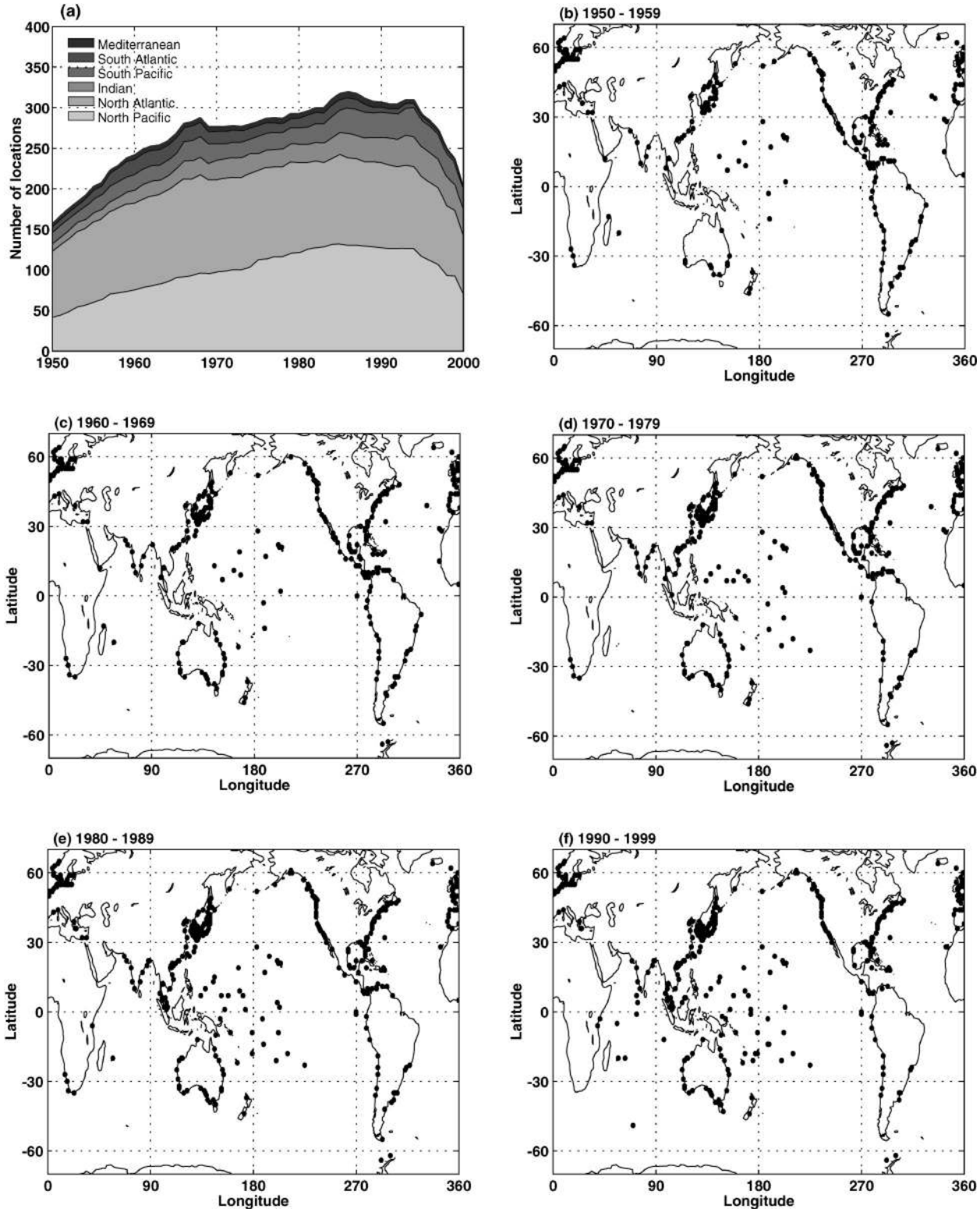

FIG. 1. Tide gauge distributions. (a) Number of tide gauge locations used for the period 1950–2000 for the various ocean basins. The regional distribution of tide gauges for the five decades: (b) the 1950s, (c) the 1960s, (d) the 1970s, (e) the 1980s, and (f) the 1990s.

and the Lambeck models adopt consistent forms of the sea level equation that are extended from traditional GIA theory (Farrell and Clark 1976) to include effects of loading-induced changes in earth rotation and improved treatment of evolving shorelines (Milne et al. 1999; Lambeck and Johnston 1998; Lambeck et al. 2003; Mitrovica et al. 2001a; Mitrovica 2003).

The Mitrovica GIA model is characterized by an elastic lithosphere of thickness 95 km, and isoviscous upper- and lower-mantle regions of viscosity 5×10^{20} Pa s and 5×10^{21} Pa s, respectively (the boundary between the regions is at 670-km depth). This viscosity model is among a class of models favored in several GIA applications, including analyses of tide gauge trends along the U.S. east coast (Davis and Mitrovica 1996) and GPS observations in Fennoscandia (Milne et al. 2001). The ice history for the Mitrovica model is based on the so-called ICE-3G global deglaciation model (Tushingham and Peltier 1991), with two noteworthy differences. First, we augment this history by including a glaciation phase and several previous glacial cycles. Furthermore, we replace the Fennoscandian component of this model with the recent history inferred by Lambeck et al. (1998b).

The Lambeck model is similarly characterized by a three-layer viscous parameterization of the mantle but with an elastic thickness for the lithosphere of 65 km, an upper mantle viscosity of 2×10^{20} Pa s, and a lower mantle viscosity of 2×10^{22} Pa s. These parameters describe well the rebound at continental margins away from the glacially loaded shields of North America and Scandinavia (Lambeck 2002; Lambeck and Chappell 2001) but higher upper-mantle viscosity values are required for these latter areas (e.g., Lambeck et al. 1998a). In the absence of a rebound model with laterally variable mantle parameters, the former values are used in this model for all sites. The ice sheet models for Scandinavia and Arctic Europe, and to a lesser degree for Antarctica, have been inferred from the inversion of the rebound data. For North America, different glaciological models have been used, scaled in amplitude such that the change in total global ice volume change is consistent with the observed eustatic sea level change during the last glacial cycle.

We also used the ICE-4G VM2 model described by Peltier (2001). The GIA corrections are from the CD-ROM included with the book by Douglas et al. (2001).

Unless stated otherwise, all results quoted are for the Mitrovica model.

b. The TOPEX/Poseidon satellite altimeter dataset

To estimate the global covariance structure of sea level variability, we use the TOPEX/Poseidon along-track altimeter data from the Merged Geophysical Data records for January 1993–December 2001 (cycles 11–342, 108 months). All standard corrections recommended by Benada (1997) were applied. In addition, the TOPEX altimeter internal calibration estimates (Hayne et al. 1994), a correction for a long-term drift in the TOPEX/Poseidon water vapour correction (Keihm et al. 2000), and the estimated drift [by comparison of the altimeter surface heights to tide-gauge data (Mitchum 1998, 2000)] were applied. The along-track data were also used to compute global mean sea level using an equal-area weighting (Nerem 1995).

As we are interested in the larger space- and time-scale phenomena, cycle-by-cycle (9.92 days) estimates of sea level on a $1^\circ \times 1^\circ$ grid were obtained by applying a Gaussian filter, with length scale of 300 km applied over a square with sides of 800 km, to the along-track data. The data were further averaged into monthly bins.

Because open-ocean sea level responds to perturbations in atmospheric pressure in an almost isostatic fashion, we account for the atmospheric pressure influence on sea level data by using an inverted barometer correction. This approach minimizes the ''noise'' in the large-scale variability of the altimeter dataset as a result of atmospheric pressure variations. Before applying the inverted barometer correction, the atmospheric pressures were adjusted so that their integral over the global oceans remains constant to ensure that no artificial signal in global mean sea level is introduced (Minster et al. 1999).

c. The atmospheric pressure dataset

Coastal sea level responds to atmospheric pressure and wind perturbations in the coastal region as well as to large-scale offshore forcing. This direct response to local atmospheric pressure forcing is almost isostatic in many circumstances and most of the apparent nonisostatic sea level variability comes from winds in the coastal region. In order to reduce the ''noise'' related to regional phenomena in the tide gauge data, we apply the inverted barometric correction. Perhaps, a more important reason for correcting the tide gauge data for variations in atmospheric pressure relates to the lack of global coverage of the former. Changes over time in atmospheric pressure patterns would redistribute sea level but with a sparse network of tide gauges this could easily be misinterpreted as a change in global sea level. We use the atmospheric pressure from the National Centers for Environmental Prediction–National Center for Atmospheric Research (NCEP–NCAR) 50-yr reanalysis (Kistler et al. 2001) provided by the National Oceanic and Atmospheric Administration–Cooperative Institute for Research in Environmental Sciences (NOAA–CIRES) Climate Diagnostics Center, Boulder, Colorado, from their Web site (http://www.cdc.noaa.gov/). Before applying the inverted barometer correction, the atmospheric pressures were adjusted so that their integral over the global oceans remains constant.

3. The analysis approach

Our approach relies on resolving large-scale ocean variability by using as many tide gauges as possible to estimate the global distribution of sea level for each month/year between 1950 and 2000. We use sea surface height anomaly satellite altimeter data to estimate the global covariance structure as expressed in empirical orthogonal functions (EOFs). We then estimate the amplitude of these EOFs by using the relatively sparse but longer tide gauge records. The estimated (reconstructed) global distribution of sea level for each month is obtained as the sum of these EOFs.

a. Methodology

A singular value decomposition is used to determine the singular values and singular vectors of the data matrix $\mathbf{H}$; that is,

$$\mathbf{H} = \mathbf{USV}^{\mathrm{T}}, \tag{1}$$

where the columns of $\mathbf{U}$ are the orthonormal spatial eigenvectors (EOFs), the rows of $\mathbf{V}^{\mathrm{T}}$ are the orthonormal time series of the amplitudes of the modes for each time step, and $\mathbf{S}$ is a diagonal matrix of the singular values of $\mathbf{H}$.

The lower-order EOFs explain more of the variance and contain the largest spatial scales. The higher-order EOFs tend to represent smaller spatial scale structures that are increasingly affected by noise in the data and their amplitudes are increasingly difficult to determine from the sparse spatial set of tide gauges. An efficient reconstruction of the observed sea surface height ($\mathbf{H}^{\mathrm{o}}$) anomaly fields is accomplished by exploiting the covariance structure of the observed data on a global scale and including only the lowest M EOFs in the reconstruction. (Here we use values of M of 10, 15, 20, 25, and 30.) The reconstructed sea surface height anomaly fields ($\mathbf{H}^{\mathrm{r}}$) is then

$$\mathbf{H}^{\mathrm{r}}(x, y, t) = \mathbf{U}^{\mathrm{r}}(x, y)\boldsymbol{\alpha}(t), \tag{2}$$

where $\mathbf{U}^{\mathrm{r}}$ includes only the leading EOFs and $\boldsymbol{\alpha}(t)$ is the time series of the amplitudes of these EOFs. Following Kaplan et al. (2000), for each month of the solution, the amplitudes of the modes are found by minimizing the cost function:

$$\mathbf{S}(\alpha) = (\mathbf{KU}^{\mathrm{r}}\alpha - \mathbf{H}^{\mathrm{o}})^{\mathrm{T}}\mathbf{M}^{-1}(\mathbf{KU}^{\mathrm{r}}\alpha - \mathbf{H}^{\mathrm{o}}) + \boldsymbol{\alpha}^{\mathrm{T}}\boldsymbol{\Lambda}\boldsymbol{\alpha}, \tag{3}$$

where $\mathbf{H}^{\mathrm{o}}$ are the tide-gauge-observed sea surface heights, $\mathbf{K}$ is a sampling operator equal to 1 when and where tide gauge data are available and 0 otherwise, and $\boldsymbol{\Lambda}$ is a diagonal matrix of the eigenvalues of the covariance matrix. Individual eigenvalues are related to the singular values in (1) by $\lambda_i = s_i^2/n$ [where n is the number of grid points; see von Storch and Zwiers (1999, p. 301)]; $\mathbf{M}$ is the error covariance matrix, given by

$$\mathbf{M} = \mathbf{R} + \mathbf{KU}'\boldsymbol{\Lambda}'\mathbf{U}'^{\mathrm{T}}\mathbf{K}^{\mathrm{T}}. \tag{4}$$

Here, $\mathbf{R}$ is the variance of the instrumental error, and the second term on the right-hand side represents the errors of omission introduced by deleting higher-order EOFs in the reconstruction. The prime indicates matrices of the omitted eigenvectors and eigenvalues. The main results given here are estimated by minimizing the cost function given in (3) [i.e., using the Kaplan et al. (2000) approach]. The benefits of this approach are that it is an optimal solution given known errors in the data and that it permits error estimates to be made. Following Kaplan, we refer to this as the optimal interpolation (OI) solution.

We test the robustness of the results by also applying the projection technique used by Smith et al. (1996) for mapping sea surface temperatures and by Chambers et al. (2002) for reconstructing sea surface height variability. In this approach, the cost function omits the second term in (3) and $\mathbf{M}$ is replaced by the identity matrix. The vectors $\mathbf{U}^{\mathrm{r}}$ are also rescaled by Smith et al. (1996) such that in (3) $\mathbf{U}^{\mathrm{r}}$ is effectively replaced by $\mathbf{U}^{\mathrm{r}}\boldsymbol{\Lambda}$. The minimization of this modified cost function may result in a noisy solution and it is often valuable to add a second term to the cost function $\boldsymbol{\epsilon}^2\boldsymbol{\alpha}^{\mathrm{T}}\boldsymbol{\alpha}$, where $\boldsymbol{\epsilon}^2$ is a (usually small) weighting factor that determines the relative importance of the prediction error versus the solution length [ridge analysis in the terminology of Menke (1989, p. 52)]. In this case, the cost function becomes

$$\mathbf{S}(\alpha) = (\mathbf{KU}^{\mathrm{r}}\alpha - \mathbf{H}^{\mathrm{o}})^{\mathrm{T}}(\mathbf{KU}^{\mathrm{r}}\alpha - \mathbf{H}^{\mathrm{o}}) + \boldsymbol{\epsilon}^2\boldsymbol{\alpha}^{\mathrm{T}}\boldsymbol{\alpha}. \tag{5}$$

In contrast to the Kaplan et al. (2000) approach, in the projection method, $\boldsymbol{\epsilon}^2$ is an arbitrary parameter and ridge analysis does not give ''true'' error estimates.

There are two further difficulties we face in reconstructing historical sea levels. First, the tide gauge measurements are all made relative to their own local datum rather than a single consistent datum. To eliminate the reliance on unknown datums, we consider the change in height between adjacent time steps. In (2), the EOFs are functions of space only and the amplitudes are functions of time only. Thus for adjacent times t_n and t_{n+1}, we can rewrite (2) as

$$\mathbf{H}^{\mathrm{r}}(x, y, t_{n+1}) - \mathbf{H}^{\mathrm{r}}(x, y, t_n) = \mathbf{U}^{\mathrm{r}}(x, y)[\boldsymbol{\alpha}(t_{n+1}) - \boldsymbol{\alpha}(t_n)]. \tag{6}$$

We then minimize the cost function for the observed change in height, thus estimating the change in the amplitude of the EOFs between each time step. This approach introduces an arbitrary constant for each EOF amplitude. We choose this constant by setting the average amplitude of each EOF equal to the average amplitude of the corresponding EOF in the TOPEX/Poseidon altimeter data (over the common period). We then integrate backward in time from December 2000 to January 1950.

The second difficulty is that in determining the EOFs from the altimeter data, we have removed the mean from the altimeter data. However, over time, mean sea level

may change considerably as the mass and volume of the ocean changes. The representation of a uniform increase is poorly represented by the limited number of EOFs available for the solution. We allow for this possibility by adding an additional constant, essentially representing an EOF (called EOF0 here) that is just a constant height (in space), and then solving for the amplitude of EOF0 in the minimization of the cost function. To separate any change in mean level from a redistribution in sea level, we set the area-averaged values of each of the remaining EOFs to 0 and renormalize the EOFs to unit amplitude. This is only a very small adjustment to the EOFs.

Prior to computing the EOFs, we remove a global-average sea level trend from the altimeter data, the inverted barometer correction, and estimates of the annual and semiannual sea level signals from both the satellite altimeter and tide gauge datasets. To test the robustness of the results we also complete the calculations by not applying the inverted barometer correction and the seasonal signal to both the altimeter and tide gauge datasets.

b. The seasonal cycle

The seasonal cycle in sea level accounts for over a third of the total large-scale sea level variance. Our focus is on the interannual and longer-term variability and thus we prefer to use the degrees of freedom available to represent the longer-term variability rather than seasonal signals. Also, many of the tide gauges we use in the reconstruction are from coastal locations and are likely to be affected by local and regional seasonal variability. We therefore remove the seasonal cycle from both the tide gauges and altimeter datasets in most of the calculations. With 9 yr of global altimeter data, estimates of the seasonal cycle are reasonably robust. The computed annual amplitudes and phases from the TOPEX/Poseidon data (not shown) are qualitatively similar to the estimates of Stammer (1997) from 3 yr of TOPEX/Poseidon data (1993–95) and will not be discussed here. For a discussion of the annual signals, particularly the wind-driven maxima in the equatorial regions, see Fu and Chelton (2001).

c. Definition of empirical orthogonal functions

The spatial structure of empirical orthogonal functions is sensitive to noise in the observational dataset. For this reason, we use the longest TOPEX/Poseidon dataset available, that is, the 9 yr of data available from January 1993 to December 2001 inclusive (we omit the first 10 cycles of TOPEX/Poseidon data). This is somewhat less than the 12 yr of data used by Smith et al. (1996) for estimating global sea surface temperature variations and substantially less than the longer time series used by Kaplan et al. (1997, 1998, 2000) for sea surface temperatures and atmospheric pressure reconstructions. However, as global coverage of sea surface height is only available for the recent satellite altimeter period, we are forced to use the EOF spatial structures determined from the TOPEX/Poseidon data for the longer period of the sea level reconstruction prior to the availability of satellite data. As an alternative, we could choose to determine the EOFs from numerical model results but since our purpose is to establish independent assessments against which models can be tested, we choose not to pursue this option here.

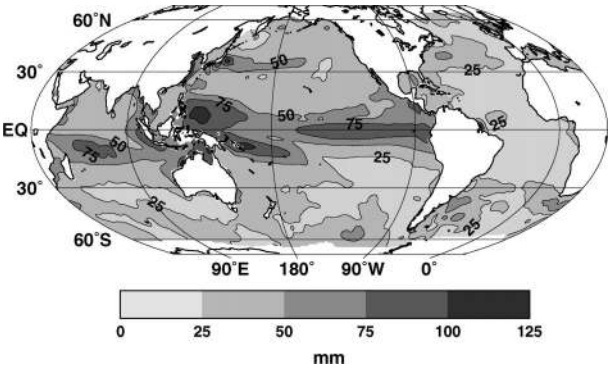

FIG. 2. The standard deviation (mm) of the TOPEX/Poseidon satellite altimeter data after removal of the annual and semiannual signals and a linear trend in globally averaged sea level. The contour interval is 25 mm.

The global-averaged standard deviation of the TOPEX/Poseidon sea surface height fields after removal of the seasonal signal is 38 mm (Fig. 2). The largest variability is in the equatorial Pacific in the region of the cold tongue along the equator east of the date line (standard deviation of about 90 mm) and two regions in the western Pacific at latitudes of about 6°–7°N and S (peaking at about 100 mm). There is also large variability in the eastern equatorial Indian Ocean and in a band across the Indian Ocean at latitudes of 5°–15°S, in the western boundary current regions, and in the Southern Ocean. In much of the rest of the ocean, the large-scale variability on monthly and longer time scales is less than 30 mm. The largest surface height signals occur during the 1997–98 ENSO event in the Pacific (Fig. 3).

We use TOPEX/Poseidon EOFs defined on a regular $1^\circ \times 1^\circ$ grid. To avoid overemphasis of the high latitudes, we use area-weighted altimeter heights in defining EOFs and in determining their amplitude from the tide gauges. The first EOFs computed after removing a global average trend, the inverted barometer effect, and the seasonal signal from the altimeter data clearly show the influence of ENSO-like events (Fig. 4). EOF 1 accounts for 38.9% of the variance and is clearly related to ENSO. It has a dipole structure in the equatorial Pacific, and secondary peaks in the western Indian Ocean and the Southern Ocean. EOF2, -3, and -4 account for 10.7%, 6.8%, and 3.9% of the variance, respectively, and show an increasingly complex spatial structure. Note that for the higher-order modes there is some small-scale structure (e.g., in the Agulhas Current region south of Africa

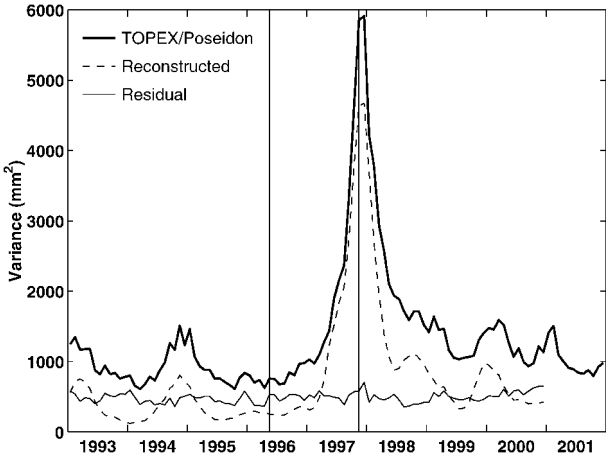

FIG. 3. The temporal (monthly values) evolution of the variance (mm^2) in the TOPEX/Poseidon satellite altimeter data after removal of the annual and semiannual signals and a linear trend in globally averaged sea level. Also shown are the variance of the reconstructed time series and the residual variance. The vertical lines indicate May 1996 and Nov 1997. Reconstructions for these periods are shown in Fig. 7.

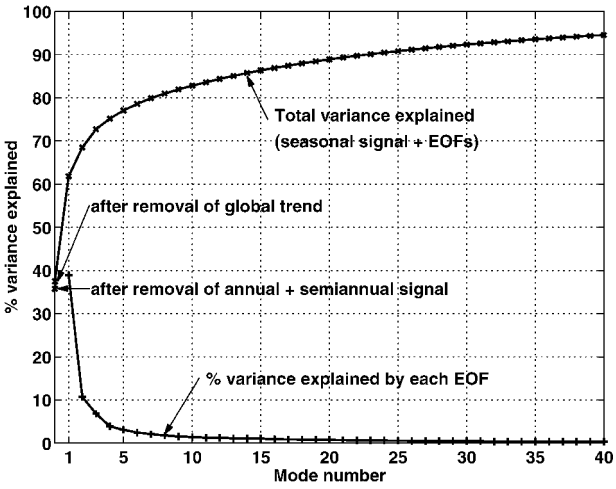

FIG. 5. The variance of the TOPEX/Poseidon satellite altimeter data explained by the sum of the annual and semiannual signals, a global average trend in sea level, and the sum of EOFs, plotted as a function of EOF number. The percentage variance explained by each EOF after removal of the seasonal signal is also shown.

in modes 3 and 4) indicating that a longer time series is required for robustly determining their spatial structure. If no inverted barometer correction is applied to the altimeter data, the lower-order modes account for a slightly reduced percentage of the variance but their spatial structure stays qualitatively the same. Excluding sections of the TOPEX/Poseidon record, including the 1997–98 ENSO event, from our analysis does not qualitatively change the spatial structure of the EOFs and there is little impact on our final results (see section 5).

The percentage variance explained by each of the EOFs decreases rapidly (Fig. 5). The percentage vari-

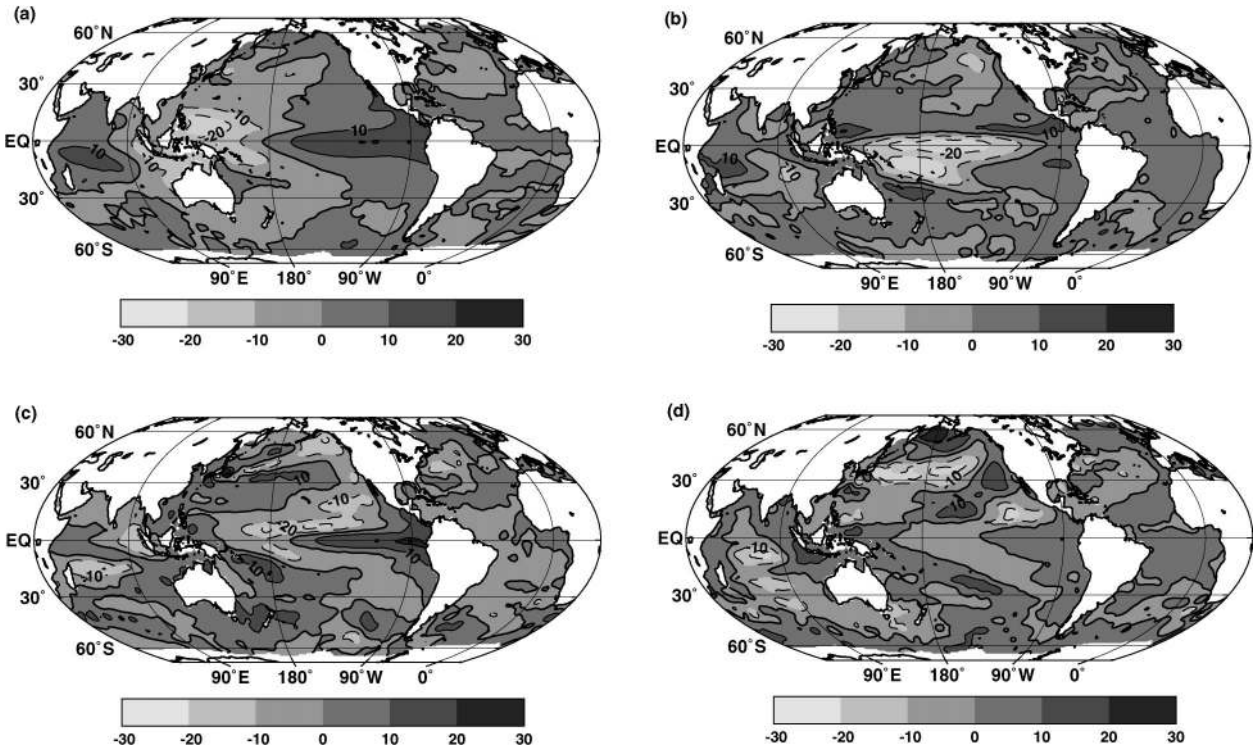

FIG. 4. The first four EOFs of the TOPEX/Poseidon satellite altimeter data after removal of the annual and semiannual signals and a linear trend in globally averaged sea level. (a)–(d) EOFs 1–4 account for 38.9%, 10.7%, 6.8%, and 3.9% of the variance, respectively.

ance explained by the sum of the seasonal signal (35.8%), a constant global average trend (1.8%), and the progressive sum of the EOFs (upper curve) increases slowly as the number of EOFs included increases. It reaches almost 90% of the total signal for 20 EOFs. The sum of the first 20 EOFs explains more than 80% of the nonseasonal signal.

d. Selection of reconstruction parameters in the cost functions

We reconstruct the global sea level fields using (2) with the time evolution of the amplitudes of the EOFs (see Fig. 14 below) determined from the tide gauge data. However, to complete the solution, we need to select the number of EOFs to retain and specify instrumental error in the cost function of (3) [or the relative weighting of the tide gauge residuals versus prediction error in the cost function of (5)].

To test the significance of increasing the number of EOFs, we compare the reduction in residual variance for the reduction in degrees of freedom with what would be expected if we were simply fitting random noise. We first use the lowest 5 EOFs (plus our constant, EOF0), then 10, 15, 20, and finally 25 EOFs. We find that the reduction in variance is significant (using the *F* test) at the 99% confidence level up to 20 EOFs. The first 10 EOFs (plus EOF0) reduce the residual tide gauge variance from 2692 to 1722 mm^2, that is, a reduction of almost 90 mm^2 per degree of freedom. Using a further 10 EOFs reduces the variance by a further 353 mm^2, 35 mm^2 per degree of freedom. However, increasing the EOFs from 20 to 25 results in an average reduction of variance of only about 10 mm^2 per degree of freedom, approaching the value expected for fitting random noise.

These results indicate that a choice of 20 EOFs (plus EOF0) is a satisfactory compromise between reducing the residual variance and not introducing random noise into the reconstructed fields. A choice of 10 EOFs (as used by Chambers et al. 2002) or possibly 30 EOFs would be almost as satisfactory.

For the instrumental error between subsequent monthly tide gauge values, we chose 4 mm, a value consistent with the expected uncertainty in estimates of monthly average sea level from tide gauges (Pugh 1987, p. 303). As the error estimate is decreased, the energy (sum of the variance of the EOF amplitudes) in the solution increases and the residual variance at the tide gauges increases. As the error estimate is increased beyond the specified value, the energy of the solution decreases slowly and the residual variance again increases.

4. Reconstructed sea level for 1993–2000

As a partial test of the ability of the reconstructions to resolve the temporal evolution of the spatial fields, we compare them with the TOPEX/Poseidon altimeter data. This is not a completely independent test because although the amplitude of the EOFs was determined from the tide gauge data, the spatial structures of the EOFs were determined from the altimeter data.

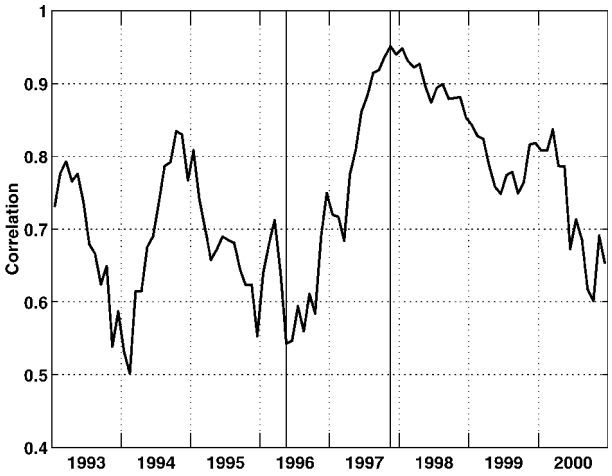

FIG. 6. The monthly area-averaged correlation between the reconstructed fields and the TOPEX/Poseidon satellite altimeter data after removal of the annual and semiannual signals and a linear trend in globally averaged sea level. The vertical lines indicate May 1996 and Nov 1997. Reconstructions for these periods are shown in Fig. 7.

The sensitivity of the results has been explored by a large number of reconstructions and the salient points are discussed below. The global-averaged variance of the reconstructed signal is about 64% of the global-averaged variance of the TOPEX/Poseidon data. It has a very similar temporal evolution (Fig. 3). In between the peaks in variability, the global average variance falls to values of about 200–300 mm^2. In contrast to the temporal evolution of the reconstructed variance, the residual variance is 43% of the altimeter variance and oscillates about a value of 540 mm^2. This would appear to be a global-averaged noise floor to our reconstructions of about 23 mm. Note that neither the mapped TOPEX/Poseidon fields used here nor the reconstructions capture the westward-propagating Rossby waves, which are often of smaller spatial scale (see, e.g., Fig. 12 of Fu and Chelton 2001). The area-averaged correlation (Fig. 6) between the reconstructed and satellite fields peaks at about 0.95 in late 1997. Even when the observed and reconstructed fields have a minimum in mid-1996 and the residual variance is larger than the reconstructed variance, the correlation remains above a value of 0.5.

Sensitivity tests indicate the residual variance can be decreased slightly by increasing the number of EOFs. If the inverted barometer correction is not applied, the altimeter, and the reconstructed and the residual variances, all increase and the residual variance expressed as a percentage of the altimeter variance increases slightly. If the seasonal signals are not removed separately, the correlation between the reconstructed and altimeter fields increases (as a result of reproducing the annual signal) but the residual variance increases.

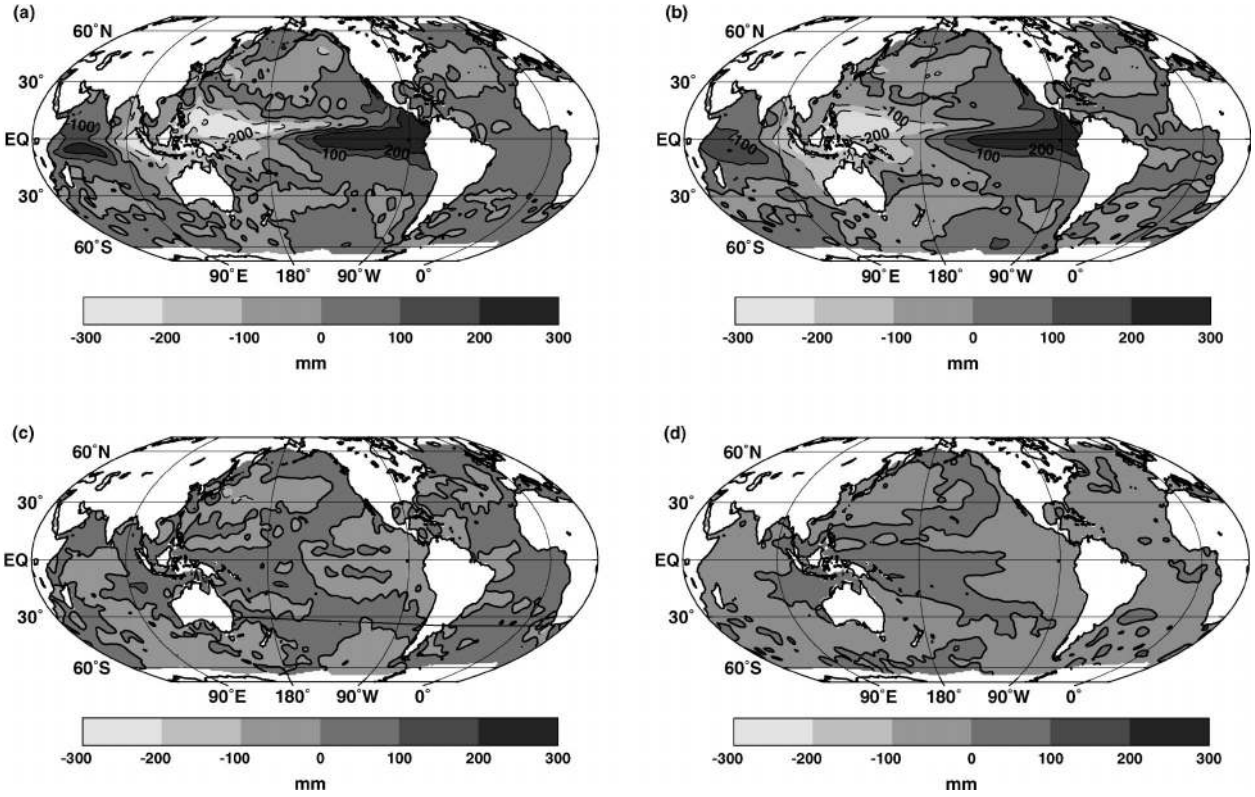

FIG. 7. The sea level field for (a) Nov 1997 and (c) May 1996, as observed by the TOPEX/Poseidon satellite altimeter data after removal of the annual and semiannual signals and a linear trend in globally averaged sea level and (b), (d) as reconstructed from the tide gauge data. The 0 contour is shown as bold, the contour interval is 100 mm, and negative contours are dashed.

We show comparisons of the spatial distribution of the surface height fields from the reconstruction with that observed from TOPEX/Poseidon for two particular time periods: November 1997 at the height of the 1997–98 El Niño–Southern Oscillation event when the observed and reconstructed variances are large (Fig. 3) and well correlated (Fig. 6), and May 1996 when the observed and reconstructed variances are small and the correlation between the two fields is at a minimum. For November 1997 (Figs. 7a,b), the two fields are remarkably similar, reflecting their high correlation of 0.95. The main difference is that the observed field is of slightly larger magnitude and contains more high-frequency spatial structure than is present in the reconstructions. For May 1996 (Figs. 7c,d), the correlation of the two fields is lower (0.56) and both the TOPEX/Poseidon and the reconstructed fields are weak. However, the main features are qualitatively similar in the two fields.

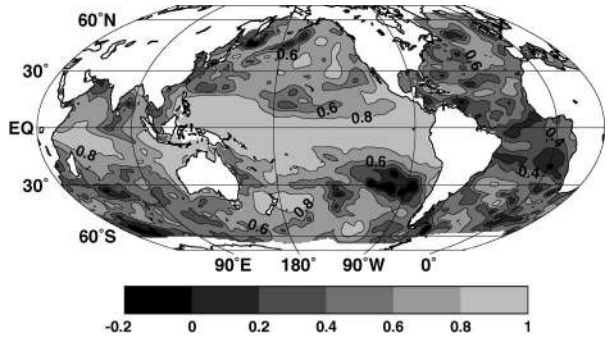

FIG. 8. The spatial distribution of the correlation between the TOPEX/Poseidon satellite altimeter data (after removal of the annual and semiannual signals and a linear trend in globally averaged sea level) and the reconstructed fields over the period Jan 1993–Dec 2000. The contour interval is 0.2.

The spatial distribution of the correlation between the fields (Fig. 8) over the eight years 1993–2000 has a global area-weighted average of 0.60. In the tropical Pacific and Indian Ocean, the correlation is above 0.9. This reflects the dominance of the low-order EOFs and the strong variance associated with the large ENSO signal of 1997–98. At higher latitudes, the correlation is more variable, with a few negative values, particularly in the areas where the large-scale variability is small. These negative values probably represent variable eddy structures affecting both the TOPEX/Poseidon fields and the EOFs.

As one of our main goals is to estimate any pattern in the regional variation of sea level rise, we compare the reconstructed trends with the TOPEX/Poseidon trends over the global oceans. For the short period when

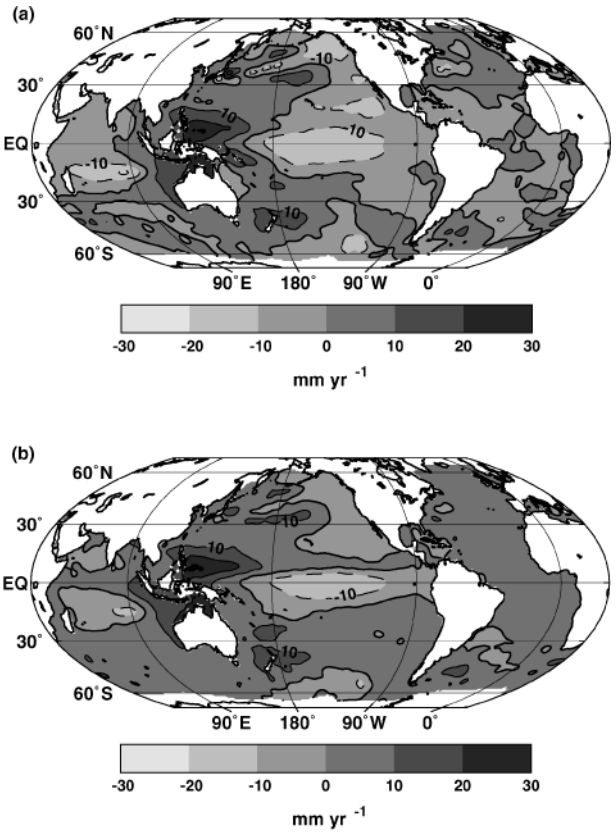

FIG. 9. The regional distribution of sea level rise (mm yr^{-1}) between Jan 1993 and Dec 2000 as evaluated from (a) the TOPEX/Poseidon satellite altimeter data and (b) the reconstructed sea level fields. The contour interval is 10 mm yr^{-1}, the 0 contour is bold, and the negative contours are dashed.

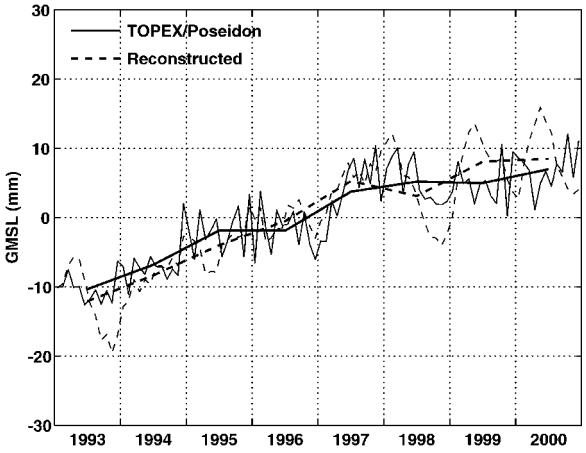

FIG. 10. Global-averaged sea level between Jan 1993 and Dec 2000 as evaluated from TOPEX/Poseidon satellite altimeter data (solid lines) and from the reconstructed sea level fields using the tide gauge data (dashed lines). The monthly data are shown by the thin lines and the yearly averaged data by the thick lines.

TOPEX/Poseidon data are available, the regional trends mostly reflect natural climate variability and as a result the regional trends are large, up to ± 25 mm yr^{-1}. The observed and reconstructed patterns (Fig. 9) are remarkably similar, the area-weighted correlation between the trends is high (0.92), and the area-weighted variance of the residual trends is only 5.6 mm^2 yr^{-2}, compared with the variance in the TOPEX/Poseidon trends of 37.0 mm^2 yr^{-2}.

Comparison of the global area-averaged mean sea level is a demanding test of both the satellite observations and the reconstructions as small biases in either dataset will affect the results. The TOPEX/Poseidon global mean sea level measurements are critically dependent on the calibration of the total system using tide gauge observations (Nerem and Mitchum 2001). As most gauges do not yet have adequate independent estimates of terrestrial land motions, Nerem and Mitchum (2001) quote relatively large error bars, ± 1.3 mm yr^{-1}, for their estimate of the observed rise of 2.5 mm yr^{-1} over the 1992–98 period.

For the reconstructions, the rate of eustatic global mean sea level rise for the 1993–2000 period is 2.9 mm yr^{-1} with the inverted barometer correction applied (Fig. 10) and 3.2 mm yr^{-1} if the inverted barometer correction is not applied. Our estimate of the TOPEX/Poseidon global mean sea level rise (cf. with the earth's center of mass) over the same period is 2.6 mm yr^{-1} if the inverted barometer correction is applied and 2.7 mm yr^{-1} if the inverted barometer correction is not applied. We estimate the error bars on all of these rates of rise over the period 1993–2000 to be ± 0.7 mm yr^{-1}. The rms difference between the area-averaged global sea level from the reconstruction and the altimeter dataset is 4.6 mm for the monthly data and 2.0 mm for the annual averaged data. Note that the reconstructions are not relative to the center of mass of the earth, as are the altimeter data. Therefore, our reconstructed global-average sea level rate will differ from the altimeter-inferred rate by an amount equal to the mean vertical displacement rate of the solid surface. If GIA dominates the latter, then TMNLM have shown that the difference will range from 0.2 to 0.5 mm yr^{-1} (depending on the adopted GIA model), with the eustatic rate being higher. This is in accord with our two estimates cited above.

5. Reconstructed sea level for 1950–2000

a. Tide gauge reconstructions

The island and coastal tide gauge records are monthly averages and contain contributions from many regional and coastal phenomena (e.g., wind-forced coastal trapped waves, local flooding events) as well as the large-scale climate-related phenomena we are attempting to recapture in the present analysis. The observed average variance of the monthly tide gauge data is 2710 mm^2 (after removal of the seasonal signal and correcting for atmospheric pressure perturbations). For the Kaplan optimal interpolation method, the variance in the re-

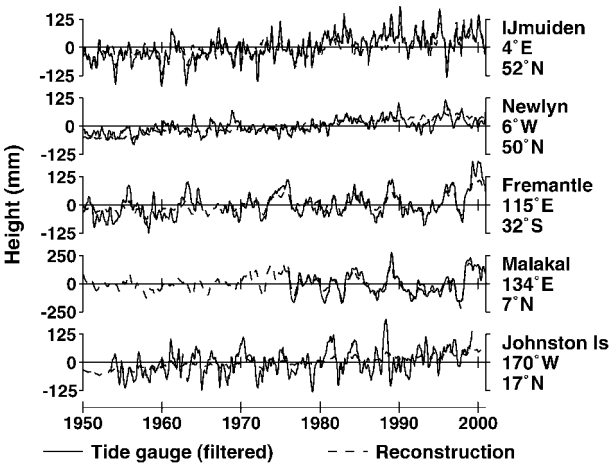

FIG. 11. Observed and reconstructed sea surface heights for selected locations.

constructed signal is 1297 mm^2 and the residual variance is 1369 mm^2, or 50.5% of the observed variance.

To illustrate the strengths and weaknesses of the reconstruction (and the tide gauge dataset itself), we present and briefly discuss examples that illustrate cases where the reconstruction reproduces the observed signal well and cases where the variability is not captured well but the mean trend is reproduced (Fig. 11). We offer the following comments on the individual records.

- In the North Sea region there are many long records with considerable variability. IJmuiden is a typical example from the European north coast where much of the variability and the trend are well reproduced.
- Newlyn is a long record from the southwestern United Kingdom. In contrast to the North Sea region, the variability is small and the amplitude of the reconstructed trend is similar to the tide gauge trend.
- Fremantle, on the Australian west coast, is a long record with significant ENSO-related variability. This variability and the trend are well reproduced.
- Malakal in the equatorial Pacific is one of the most energetic records in the dataset. Much of the variability, related to ENSO events, is well reproduced. As a result, the residual variance is less than 20% of the observed variance.
- Johnston Island in the Pacific has large interannual variance that is not reproduced. TOPEX/Poseidon data (Fu and Chelton 2001) indicate this variance is related to Rossby waves. These will be largely removed by our low-pass filter and will not be represented in the low-order EOFs. They are features we are not attempting to reproduce. However, the trend at Johnston Island is well reproduced.

b. Global averaged sea level rise

The estimated global mean rate of sea level rise over the period 1950–2000 computed for the optimal choice

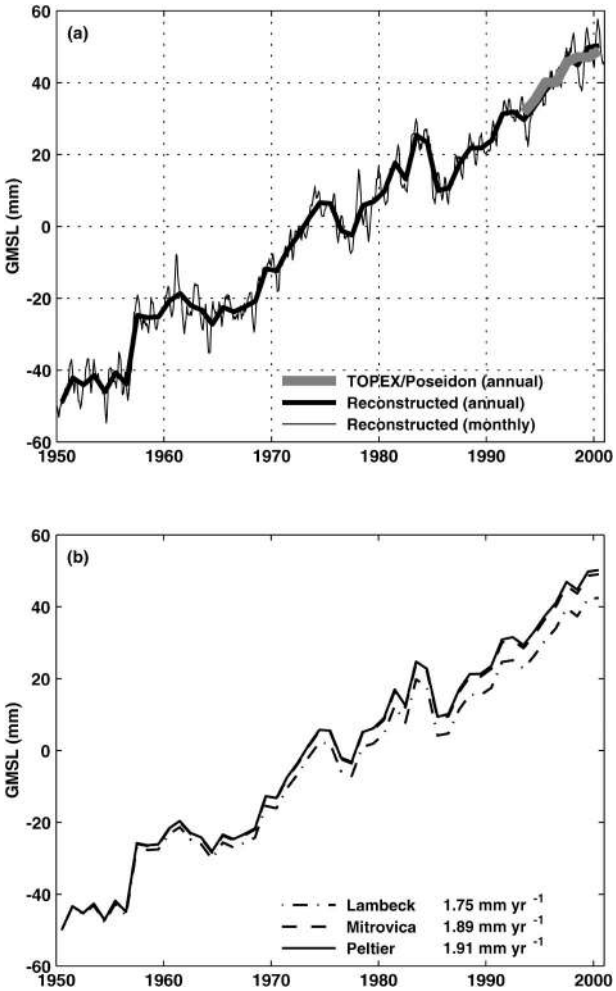

FIG. 12. Global-averaged sea level between Jan 1950 and Dec 2000 from the reconstructed sea level fields. (a) Monthly and yearly average reconstructed values using the Mitrovica GIA model are shown. The global mean sea level from the TOPEX/Poseidon satellite is also shown. (b) Yearly average values of global mean sea level for the Lambeck, Mitrovica, and Peltier GIA model corrections.

of parameters and using the Lambeck, Mitrovica, and Peltier GIA corrections are 1.75, 1.89, and 1.91 mm yr^{-1}, respectively (Fig. 12). The decadal variability alone leads to an uncertainty in the rate of sea level rise of less than $\pm$0.1 mm yr^{-1}. Differences between these three estimates are a result of the different earth models used, different ice models, and possibly differences in the numerical solutions of the glacio–hydro–isostatic sea level equations (see Mitrovica 2003). Agreement between the isostatic corrections for the individual sites is generally good away from the former ice margins where the details of the ice sheet models are not important. Comparison of the three models gives the mean difference in GIA corrections south of 20°N of less than 0.1 mm yr^{-1} and a standard deviation of the difference of less than 0.3 mm yr^{-1}. The Mitrovica and Lambeck results agree well for Scandinavia reflecting the fact that

the former has adopted the latter's ice model for this region. Discrepancies between the two are larger for the Atlantic coast of North America, probably the result of different rheologies used and because the Lambeck Late Glacial North American ice model may not extend sufficiently far onto the continental shelf. These differences will be discussed elsewhere but for these globally averaged solutions they are not critical.

For the optimal interpolation technique, the number of EOFs selected has no impact on the rate of sea level rise computed and very little impact on the time series of the amplitudes of the lowest EOFs. The rate of rise is weakly dependent on the specified tide gauge error. For values ranging from 3 to 5 mm, the rate of rise varies by 0.05 mm yr^{-1} and for the full range of values tested (1–8 mm), the rate of rise varies by 0.27 mm yr^{-1}. However, the extremes of these values imply unrealistic estimates of monthly mean sea level errors at individual gauges and in general result in a poorer fit to both the TOPEX/Poseidon satellite data and the tide gauge data.

We have computed formal error bars for the solution, following the technique of Kaplan. These imply an error in the rate of sea level rise of less than ± 0.1 mm yr^{-1}, a value we consider to be unrealistically low. In an attempt to estimate a more realistic error bar on the rate of rise resulting from the incomplete global coverage of tide gauges, we omitted a number of tide gauges from the reconstructions. First, we separately deleted all the gauges from each of 13 separate areas. This resulted in a range of estimates from 1.79 to 1.98 mm yr^{-1}. We then completed a series of 50 reconstructions in which we randomly rejected 20% of the tide gauge locations. The mean of the global sea level rise for the 50 runs was 0.03 mm yr^{-1} less than for the case using all gauges, and the standard deviation for the 50 runs was 0.07 mm yr^{-1}. If all of the metric tide gauges are omitted (i.e., omitting 15% of locations), the computed rate of sea level rise is 1.84 mm yr^{-1}. If only Northern Hemisphere gauges are used, the rate of sea level rise is decreased to 1.70 mm yr^{-1}.

We have also computed the rate of sea level rise by not including adjustments for atmospheric pressure variations. This results in a reduction in the rate of global-averaged sea level rise by about 0.16 mm yr^{-1}. A map of the atmospheric pressure trends adjusted such that the global ocean atmospheric pressure integral remains constant (Fig. 13) reveals that virtually all of the tide gauges included in the reconstruction are in regions of increasing atmospheric pressure, suppressing the rate of sea level rise at these locations. The average of the atmospheric pressure trends (adjusted such that the global ocean pressure integral is constant) at the tide gauge locations is about 0.2 mm yr^{-1}, explaining the difference between the two computations of global-averaged sea level rise. It seems that the more accurate procedure to estimate the global average rate of sea level rise is to include the atmospheric pressure adjustment to both the satellite and tide gauge data. Another sensitivity test was to exclude sections of the TOPEX/Poseidon record from the determination of the spatial structure of the EOFs. This resulted in changes in global mean sea level of about 0.1 mm yr^{-1} and little change in the overall pattern of sea level rise. Finally, not filtering the tide gauge data resulted in a slightly noisier time series of global mean sea level and the average trend changed by about 0.1–0.2 mm yr^{-1}.

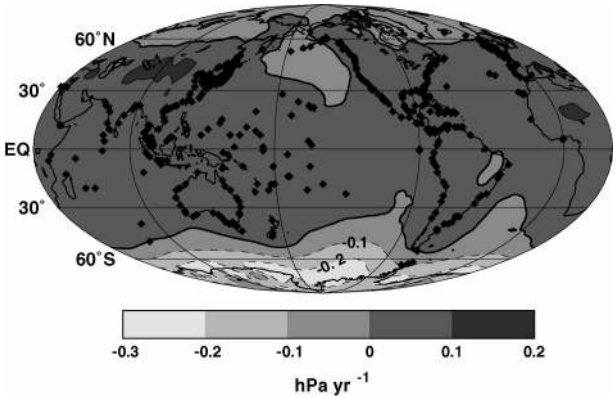

FIG. 13. Trends in the NCEP atmospheric pressure over the period Jan 1950–Dec 2000. The atmospheric pressures for each month are relative to the global ocean integral of the atmospheric pressure for that month. The locations of the tide gauges are also shown. The thick line is the 0 contour, the negative contours are dashed, and the contour interval is 0.1 hPa yr^{-1}.

As a simple test of the above reconstructions, we averaged the first differences of each of the tide gauge records (including atmospheric pressure adjustments and GIA corrections) and then integrated the differences over the 50-yr period [similar to the approach of Trupin and Wahr (1990)]. This estimate of global-averaged rate of sea level rise is 2.00 mm yr^{-1}, a little larger than the full calculations. However, the error bars on this estimate may be large since no account was taken of the regional distribution of the gauges.

Based on the above results and combining all of the error contributions, our best estimate of the rate of global averaged sea level rise is 1.8 ± 0.3 mm yr^{-1}.

c. The regional distribution of sea level rise

The regional distribution of the rate of sea level rise is determined by the change in the amplitude of the EOFs (Fig. 14). EOFs 1–4 all have a small (but nevertheless non-0) trends in amplitude during the period. Some of the higher-order modes have more consistent trends during the period.

The trends in the EOF amplitudes (and the implied global correlations) are responsible for a spatially variable rate of sea level rise (Fig. 15). The main features being the maximum rate of rise (mostly between 2 and 2.5 mm yr^{-1} but peaking at over 3 mm yr^{-1}) in the central to eastern off-equatorial Pacific, spreading north

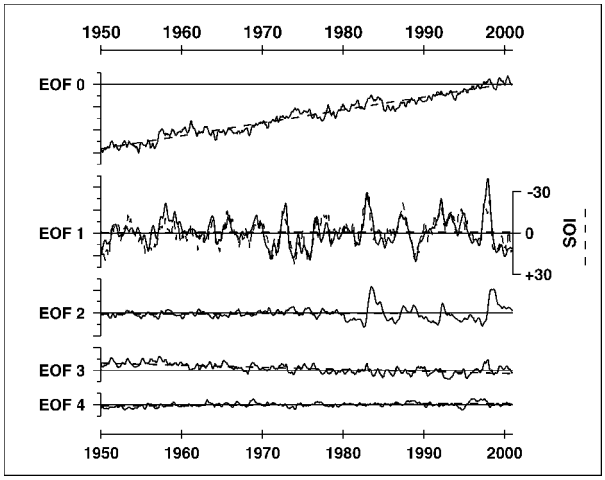

FIG. 14. The time series of EOFs 1–4 between Jan 1950 and Dec 2000 as evaluated using the tide gauge data. EOF0, representing a uniform change in sea level, is also shown. The SOI (inverted) is also plotted (dashed) with EOF1.

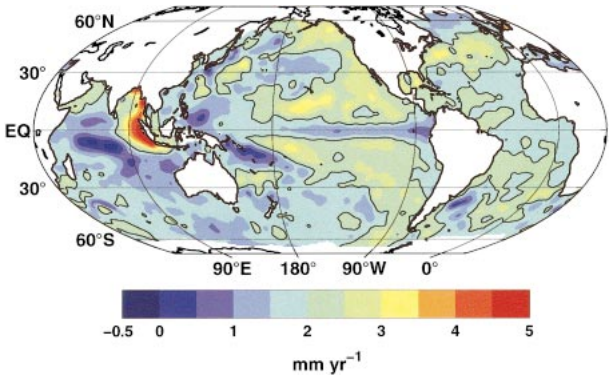

FIG. 15. The regional distribution of sea level rise between Jan 1950 and Dec 2000 from the reconstructed sea level fields using the tide gauge data. The solid line is 2.0 mm yr^{-1} and the contour interval is 0.5 mm yr^{-1}.

and south to higher latitudes. This maximum appears as a tonguelike feature wrapping around the subtropical gyres of the Pacific Ocean. This maximum is split by a minimum rate of rise (less than 1.5 mm yr^{-1}) along the equator in the eastern Pacific linking to the western Pacific as well as to the eastern Indian Ocean, including along the Australian northwest and west coast, and the central Indian Ocean. There is also a maximum rate of rise in the northeastern Indian Ocean. The minimum in rise along the northwest Australian coast is consistent with the results of Lambeck (2002). Observed smaller rates of sea level rise and indeed sea level fall off of northwestern Australia over the last few decades have been used by some to argue that global-averaged sea level is not rising at all. However, Fig. 15 puts these regional observations into a global context and allows a more realistic interpretation of the observations. For the North Atlantic Ocean, the rate of rise reaches a maximum (over 2 mm yr^{-1}) in a band running east-northeast from the U.S. east coast. The trends are lower in the east Atlantic than in the west as suggested by Woodworth et al. (1999), Lambeck et al. (1998a), and Mitrovica et al. (2001b).

The maps of sea level rise using the three GIA models (Lambeck, Mitrovica, and Peltier) are qualitatively similar, differencing by less than 0.5 mm yr^{-1} over most of the ocean. For the 50 runs, each randomly deleting 20% of the tide gauge locations, each of the maps of sea level rise were qualitatively similar, with the standard deviation of the 50 runs being less than 0.3 mm yr^{-1} for most of the ocean. The highest variation between the runs was in the tropical Pacific (values around 0.4 mm yr^{-1}) and near 10°S, 60°E in the Indian Ocean where values exceed 0.5 mm yr^{-1}.

d. Change in El Niño–Southern Oscillation conditions

Also apparent in Fig. 14 is an increase in the variance of EOF1 and -2 during the period 1950–2000 (inclusive). There is a good (negative) correlation ($r = -0.78$ at 0 lag) of EOF1 with the Southern Oscillation index, which also shows an increasing amplitude during the period. This increased variability of EOF1 and -2 implies more extreme sea level events (both high and low sea levels) in the equatorial Pacific in the last two decades. This trend is consistent with a shift to ENSO events being more frequent, persistent, and intense in the equatorial Pacific in the last two decades (Folland et al. 2001).

6. Discussion

The approach taken here is very different from most traditional attempts to estimate historical rates of sea level rise. As demonstrated by Douglas (2001) and others, individual tide gauges have annual, interannual, and decadal variability of centimeters. This variability necessitates the use of long averaging times to get stable estimates of the rate of sea level change from individual gauge records. The traditional approach has precluded the possibility of observing interannual and decadal variability of the rate of sea level change. Also, the fact that different gauges have operated over different time periods means that different estimates of the rate of twentieth century sea level rise apply for different periods, thus making the task of estimating any regional variations in the rate of rise more difficult.

Analysis of TOPEX/Poseidon satellite altimeter data has demonstrated that meaningful estimates of global-averaged mean sea level change can be made over much shorter periods than possible with tide gauges because the global satellite data account for horizontal displacements of ocean mass. Our tide gauge reconstructions estimate sea level change on a near-global ocean grid,

and as a result the variability (about a linear trend line) in our estimates of global mean sea level is less than 6.3 mm for the monthly values, an order of magnitude less than the decadal variability of centimeters in individual tide gauge records. This greatly reduced variability is similar to that seen in the short satellite record to date and suggests that the approach adopted here does effectively separate much of the internal variability of the ocean from global-averaged sea level rise.

The reconstructions accurately reproduce the monthly distribution of sea level as observed in the TOPEX/Poseidon data, particularly the strong sea level signal associated with ENSO events. As a result, the reconstructions may be valuable fields for assimilating in ocean and climate models of interannual variability. The reconstructions also reproduce the distribution in sea level rise observed by satellite. For the period 1993–2000, the reconstruction gives a rate of global-average mean sea level rise of 2.9 ± 0.7 mm yr^{-1}, agreeing well with the rise estimated from the satellite altimeter observations of 2.6 ± 0.7 mm yr^{-1}. The two estimates are virtually identical when one takes into account the expected signal from GIA-induced vertical motions of the solid surface (TMLNM).

Although the rate of sea level rise during the TOPEX/Poseidon period is greater than the average rate of rise over the 51-yr period, visual inspection and fitting a quadratic to the time series confirms there is no significant increase in the rate of rise (Fig. 12), consistent with earlier findings of Woodworth (1990) and Douglas (1992). A histogram of the trends over all 8-yr segments over the 1950–2000 period (not shown) indicates that while the trends for 1993–2000 are above the average for the whole period there have been other periods with larger trends.

The global mean sea level has maxima (compared with a linear trend) lasting several years in about 1960, 1975, and 1983 (Fig. 12) and the time series of global mean sea level is quite different from the time series of ocean thermal expansion (Antonov et al. 2002; Cabanes et al. 2001). In particular, the large variability in the ocean thermal expansion data for the 1980s–1990s [and the implied ocean heat content (Levitus et al. 2000)] is not present in the global mean sea level time series. We note that the minima in detrended global mean sea levels in about 1965, 1977, 1987, and 1994 occur a few years after volcanic eruptions and the consequent negative forcing of global climate (Ramaswamy et al. 2001).

While we find only a weak correlation of global mean sea level with the Southern Oscillation index [SOI; cf. with Nerem et al. (1999)], there is a strong correlation between the SOI and the time series of the first EOF (Fig. 14). The trend to more frequent, persistent, and intense ENSO events, as evidenced by the SOI since the mid-1970s (Folland et al. 2001), is also apparent in the first EOF. The tendency to more El Niño–like conditions in the equatorial Pacific is also revealed in observations of subsurface ocean temperatures and thus trends in surface steric height from ocean thermal expansion.

Using the historical ocean dataset of Levitus et al. (2000), Antonov et al. (2002) and Cabanes et al. (2001) find a maximum in steric sea level rise (thermal expansion alone not including other contributions to sea level rise) over the 40-yr period 1955–95 of over 2 mm yr^{-1} in the eastern equatorial Pacific and a fall in steric sea level of about 2 mm yr^{-1} in the western equatorial Pacific. While this pattern has some similarities to our results (Fig. 15), there are also significant differences. For example, the ocean thermal expansion data do not show the minimum in sea level rise along the Pacific equator.

Cabanes et al. (2001) argued on the basis of their computed pattern of ocean thermal expansion that the tide gauge locations used by Douglas (1991, 1997) result in an overestimate of the rate of sea level rise. Church (2001) cautioned against this interpretation because of the inadequate historical ocean temperature and salinity datasets for many areas of the global oceans. Our results confirm that there is a regional distribution of sea level rise. However, our estimate of global mean sea level rise is about three times the value suggested by Cabanes et al. (2001) and an average of the reconstructed sea level rise at the locations of the tide gauges used by Douglas (1997), with and without the inverted barometer correction, gives a sea level rise estimate of 2.1 and 2.2 mm yr^{-1}, versus our global average of 1.89 mm yr^{-1} (for 1950–2000). Using only Northern Hemisphere gauges in the reconstruction gives an estimate of global average rate of sea level rise of 1.70 mm yr^{-1}, slightly less than the global average rather than considerably larger as found by Cabanes et al. (2001).

Our analysis did not attempt to detect the fingerprint of the elastic response of the earth to modern glacial melting on the regional distribution of sea level rise as discussed by Mitrovica et al. (2001b). However, the minimum in sea level rise southeast of Greenland may be an indication of this effect. Our assumption that the spatial variability of eustatic sea level changes can be inferred from variability evident in altimeter data has some limitations. For example, one process contributing to both fields is GIA and recent, global maps of this ongoing adjustment (e.g., Mitrovica et al. 2001b) reveal rather distinct spatial geometries within the latitude range sampled by TOPEX/Poseidon. We hope to pursue these issues in future studies.

The first two EOFs and the SOI have a trend of increasing variance with time. This would be consistent with larger interannual variations in sea level. However, further analysis of this phenomenon, the changing relationships between the EOFs and the SOI, are beyond the scope of the present paper and will be pursued elsewhere.

Important extensions to the work of Chambers et al. (2002) that allowed us to focus on sea level trends are the use of a more robust analysis technique, the inclu-

sion of an additional constant (EOF0), and using first differences to eliminate problems of unknown datums. Of course careful quality control and the inclusion of as much data as possible remains critical. The Kaplan method results in well-behaved solutions that are characterized by very little impact on the amplitudes of the low-order EOFs as higher-order EOFs are added. We have also repeated the analyses with the projection method. Both methods give similar results but we find the projection method to be not as stable and care is required to ensure that the tide gauge time series are not ''overfitted.''

7. Conclusions

The results highlight the continuing value of the Global Sea Level Observing System (GLOSS) tide gauge network in the satellite altimeter era. Even some of the shorter tide gauge records can be of value, particularly if they are in regions with little data. Our computed rate of global averaged mean sea level rise is 1.8 $\pm$ 0.3 mm yr^{-1}. The major sources of uncertainty are the inadequate geographical distribution of tide gauges, particularly in the Southern Hemisphere; inadequate information on various geophysical signatures in the tide gauge data (glacial isostatic adjustment and tectonic activity); and the short satellite altimeter record used to estimate global sea level covariance functions. Decadal variability in sea level is observed but to date there is no detectable secular increase in the rate of sea level rise over the period 1950–2000. The results demonstrate a clear regional pattern, features of which are consistent with other known changes in the climate system as well as with previously observed regional differences in the rate of sea level rise.

Acknowledgments. This paper is a contribution to the CSIRO Climate Change Research Program. JAC was partially supported by the AusAID-funded South Pacific Sea Level and Climate Monitoring Project. NCEP–NCAR reanalysis data, provided by the NOAA–CIRES Climate Diagnostics Center, Boulder, Colorado, were acquired from their Web site (http://www.cdc.noaa.gov/).

REFERENCES

Antonov, J. I., S. Levitus, and T. P. Boyd, 2002: Steric sea level variations during 1957–1994: The importance of salinity. *J. Geophys. Res.*, **107,** 8013, doi:10.1029/2001JC000964.

Benada, J. R., 1997: PO.DAAC merged GDR (TOPEX/Poseidon) generation B user's handbook. Version 2.0. JPL PO.DAAC 068.D002, 124 pp.

Cabanes, C., A. Cazenave, and C. Le Provost, 2001: Sea level rise during the 1990s and past 40 years: New insight from satellite and in situ observations. *Science,* **294,** 840–842.

Cazenave, A., K. Dominh, L. Soudrarin, F. Ponchaut, and C. Le Provost, 1999: Sea level changes from TOPEX-POSEIDON altimetry and tide gauges and vertical crustal motions from DORIS. *Geophys. Res. Lett.,* **26,** 2077–2080.

Chambers, D. P., C. A. Melhaff, T. J. Urban, D. Fuji, and R. S. Nerem, 2002: Low-frequency variations in global mean sea level: 1950–2000. *J. Geophys. Res.,* **107,** 3026, doi:10.129/2001JC001089.

Church, J. A., 2001: How fast are sea levels rising? *Science,* **294,** 802–803.

——, J. M. Gregory, P. Huybrechts, M. Kuhn, K. Lambeck, M. T. Nhuan, D. Qin, and P. L. Woodworth, 2001: Changes in sea level. *Climate Change 2001: The Scientific Basis,* J. T. Houghton et al., Eds., Cambridge University Press, 639–694.

Davis, J. L., and J. X. Mitrovica, 1996: Glacial isostatic adjustment and the anomalous tide gauge record of eastern North America. *Nature,* **379,** 331–333.

Douglas, B. C., 1991: Global sea level rise. *J. Geophys. Res.,* **96,** 6981–6992.

——, 1992: Global sea level acceleration. *J. Geophys. Res.,* **97,** 12 699–12 706.

——, 1997: Global sea rise: A redetermination. *Surv. Geophys.,* **18,** 279–292.

——, 2001: Sea level change in the era of the recording tide gauge. *Sea Level Rise,* B. C. Douglas, M. S. Kearney, and S. P. Leatherman, Eds., International Geophysical Series, Vol. 75, Academic Press, 37–64.

——, and W. R. Peltier, 2002: The puzzle of global sea-level rise. *Phys. Today,* **55,** 35–40.

——, M. S. Kearney, and S. P. Leatherman, Eds., 2001: *Sea Level Rise*. International Geophysical Series, Vol. 75, Academic Press, 232 pp.

Dziewonski, A. M., and D. L. Anderson, 1981: Preliminary Reference Earth Model (PREM). *Phys. Earth Planet. Int.,* **25,** 297–356.

Farrell, W. E., and J. A. Clark, 1976: On postglacial sea level. *Geophys. J. Roy. Astrophys. Soc.,* **46,** 647–667.

Fleming, K., P. Johnston, D. Zwartz, Y. Yokoyama, K. Lambeck, and J. Chappell, 1998: Refining the eustatic sea-level curve since the Last Glacial Maximum using far- and intermediate-field sites. *Earth Planet. Sci. Lett.,* **163,** 327–342.

Folland, C. K., and Coauthors, 2001: Observed climate variability and change. *Climate Change 2001: The Scientific Basis,* J. T. Houghton et al., Eds., Cambridge University Press, 99–181.

Fu, L.-L., and A. Cazenave, 2001: *Satellite Altimetry and Earth Sciences.* International Geophysics Series, Vol. 69, Academic Press, 463 pp.

——, and D. B. Chelton, 2001: Large-scale ocean circulation. *Satellite Altimetry and Earth Sciences,* L. L. Fu and A. Cazenave, Eds., International Geophysical Series, Vol. 69, Academic Press, 133–169.

Gornitz, V., 1995: A comparison between recent and late Holocene sea level trends from eastern North America and other selected regions. *J. Coastal Res.,* **17,** 287–297.

Gregory, J. M., and Coauthors, 2001: Comparison of results from several AOGCMs for global and regional sea-level change 1900–2100. *Climate Dyn.,* **18,** 225–240.

Hayne, G. S., D. W. Hancock, C. L. Purdy, and P. S. Callahan, 1994: The correction for significant wave height and attitude effects in the TOPEX radar altimeter. *J. Geophys. Res.,* **99,** 24 941–24 955.

Hunter, J., R. Coleman, and D. Pugh, 2003: The sea level at Port Arthur, Tasmania, from 1841 to the present. *Geophys. Res. Lett.,* **30,** 1401, doi:10.1027/2002GL016813.

Johansson, J. M., and Coauthors, 2002: Continuous GPS measurements of postglacial adjustments in Fennoscandia 1. Geodetid results. *J. Geophys. Res.,* **107,** 2157, doi:10.1029/2001JB000400.

Kaplan, A., Y. Kushnir, M. A. Cane, and M. B. Blumenthal, 1997: Reduced space optimal analysis for historical data sets: 136 years of Atlantic sea surface temperatures. *J. Geophys. Res.,* **102,** 27 835–27 860.

——, M. A. Cane, Y. Kushnir, and A. C. Clement, 1998: Analyses of global sea surface temperatures 1856–1991. *J. Geophys. Res.,* **103,** 18 567–18 589.

——, Y. Kushnir, and M. A. Cane, 2000: Reduced space optimal interpolation of historical marine sea level pressure. *J. Climate,* **13,** 2987–3002.

Keihm, S., V. Zlotnicki, and C. Ruf, 2000: TOPEX microwave radiometer performance evaluation. *IEEE Trans. Geosci. Remote Sens.,* **38,** 1379–1386.

Kistler, R., and Coauthors, 2001: The NCEP–NCAR 50-Year Reanalysis: Monthly means CD-ROM and documentation. *Bull. Amer. Meteor. Soc.,* **82,** 247–267.

Lambeck, K., 2002: Sea-level change from mid-Holocene to recent time: An Australian example with global implications. *Ice Sheets, Sea Level and the Dynamic Earth,* J. X. Mitrovica and B. L. A. Vermeersen, Eds., Geodynamics Series, Vol. 29, 33–50.

——, and P. Johnston, 1998: The viscosity of the mantle: Evidence from analyses of glacial rebound phenonena. *The Earth's Mantle,* I. Jackson, Ed., Cambridge University Press, 461–502.

——, and E. Bard, 2000: Sea level changes along the French Mediterranean coast since the time of the last glacial maximum. *Earth Planet. Sci. Lett.,* **175,** 203–222.

——, and J. Chappell, 2001: Sea level change through the last glacial cycle. *Nature,* **292,** 679–686.

——, C. Smither, and M. Ekman, 1998a: Tests of glacial rebound models for Fennoscandinavia based on instrumental sea- and lake-level records. *Geophys. J. Int.,* **135,** 375–387.

——, —— and P. Johnston, 1998b: Sea-level change, glacial rebound and mantle viscosity for northern Europe. *Geophys. J. Int.,* **134,** 102–144.

——, A. Purcell, P. Johnston, M. Nakada, and Y. Yokoyama, 2003: Waterload definition in the glacio-hydro-isostatic sea-level equation. *Quat. Sci. Rev.,* **22,** 309–318.

Levitus, S., J. Antonov, T. P. Boyer, and C. Stephens, 2000: Warming of the World Ocean. *Science,* **287,** 2225–2229.

Menke, W., 1989: *Geophysical Data Analysis: Discrete Inverse Theory.* International Geophysics Series, Vol. 45, Academic Press, 289 pp.

Milne, G. A., J. X. Mitrovica, and J. L. Davis, 1999: Near-field hydro-isostasy: The implementation of a revised sea-level equation. *Geophys. J. Int.,* **139,** 464–482.

——, J. L. Davis, J. X. Mitrovica, H.-G. Scherneck, J. M. Johansson, M. Vermeer, and H. Koivula, 2001: Space-geodetic constraints on glacial isostatic adjustment in Fennoscandia. *Science,* **291,** 2381–2385.

Minister, J. F., A. Cazenave, Y. V. Serafini, F. Mercier, M. C. Gennero, and P. Rogel, 1999: Annual cycle in mean sea level from Topex-Poseidon and ERS-1: Inference on the global hydrological cycle. *Global Planet. Change,* **20,** 57–66.

Mitchum, G. T., 1998: Monitoring the stability of satellite altimeters with tide gauges. *J. Atmos. Oceanic Technol.,* **15,** 721–730.

——, 2000: An improved calibration of satellite altimetric height using tide gauge sea levels with adjustment for land motion. *Mar. Geod.,* **23,** 145–166.

Mitrovica, J. X., 2003: Recent controversies in predicting post-glacial sea-level change. *Quat. Sci. Rev.,* **22,** 127–133.

——, and J. L. Davis, 1995: Present-day post-glacial sea level change far from the Late Pleistocene ice sheets: Implications for recent analyses of tide gauge records. *Geophys. Res. Lett.,* **22,** 2529–2532.

——, G. A. Milne, and J. L. Davis, 2001a: Glacial isostatic adjustment on a rotating earth. *Geophys. J. Int.,* **147,** 562–578.

——, M. Tamisiea, J. L. Davis, and G. A. Milne, 2001b: Recent mass balance of polar ice sheets inferred from patterns of global sea-level change. *Nature,* **409,** 1026–1029.

Nakiboglu, S. M., and K. Lambeck, 1991: Secular sea-level change. *Glacial Isostasy, Sea Level and Mantle Rheology,* R. Sabadini, K. Lambeck, and E. Boschi, Eds., Kluwer Academic, 237–258.

Nerem, R. S., 1995: Measuring global mean sea level variations using TOPEX/Poseidon altimeter data. *J. Geophys. Res.,* **100,** 25 135–25 153.

——, and G. T. Mitchum, 2001: Sea level change. *Satellite Altimetry and Earth Sciences,* L. L. Fu and A. Cazenave, Eds., International Geophysical Series, Vol. 69, Academic Press, 329–349.

——, E. W. Leuliette, D. P. Chambers, G. T. Mitchum, and B. S. Giese, 1999: Variations in global mea sea level associated with the 1997–98 ENSO event. *Geophys. Res. Lett.,* **26,** 3005–3008.

Peltier, W. R., 1996: Global sea level rise and glacial isostatic adjustment: An analysis of data from the east coast of North America. *Geophys. Res. Lett.,* **23,** 717–720.

——, 1998: Postglacial variations in the level of the sea: Implications for climate dynamics and solid-earth physics. *Rev. Geophys.,* **36,** 603–689.

——, 2001: Global glacial isostatic adjustment and modern instrumental records of relative sea level history. *Sea Level Rise,* B. C. Douglas, M. S. Kearney, and S. P. Leatherman, Eds., International Geophysical Series, Vol. 75, Academic Press, 65–95.

Pugh, D. T., 1987: *Tides Surges and Mean Sea Level.* John Wiley and Sons, 472 pp.

Ramaswamy, V., and Coauthors, 2001: Radiative forcing of climate change. *Climate Change 2001: The Scientific Basis,* J. T. Houghton et al., Eds., Cambridge University Press, 347–416.

Smith, T. M., 2000: Tropical Pacific sea level variations (1948–98). *J. Climate,* **13,** 2757–2769.

——, R. W. Reynolds, R. E. Livezey, and D. C. Stokes, 1996: Reconstruction of historical sea surface temperatures using empirical orthogonal functions. *J. Climate,* **9,** 1403–1420.

Smith, T. S., R. E. Livezey, and S. S. Chen, 1998: An improved method for analyzing sparse and irregularly distributed SST data on a regular grid: The tropical Pacific Ocean. *J. Climate,* **11,** 1717–1729.

Stammer, D., 1997: Global characteristics of ocean variability estimated from regional TOPEX/Poseidon altimeter measurements. *J. Phys. Oceanogr.,* **27,** 1743–1769.

Trupin, A., and J. Wahr, 1990: Spectroscopic analysis of global tide gauge sea level data. *Geophys. J. Int.,* **100,** 441–453.

Tushinam, A. M., and W. R. Peltier, 1991: Ice-3G: A new global model of late Pleistocene deglaciation based upon predictions of post-glacial relative sea level change. *J. Geophys. Res.,* **96,** 4497–4523.

von Storch, H., and F. W. Zwiers, 1999: *Statistical Analysis in Climate Research.* Cambridge University Press, 484 pp.

Woodworth, P. L., 1990: A search for accelerations in records of European mean sea level. *Int. J. Climatol.,* **10,** 129–143.

——, 1999: High waters at Liverpool since 1768: The UK's longest sea level record. *Geophys. Res. Lett.,* **26,** 1589–1592.

——, and R. Player, 2003: The Permanent Service for Mean Sea Level: An update to the 21st century. *J. Coastal Res.,* **19,** 287–295.

——, M. N. Tsimplis, R. A. Flather, and I. Shennan, 1999: A review of the trends observed in British Isles mean sea level data measured by tide gauges. *Geophys. J. Int.* **136,** 651–670.

Zhen, W. Z., and R. H. Wu, 1993: Sea level changes of the world and China. *Mar. Sci. Bull.,* **12,** 95–99.